J. Condensed Matter Nucl. Sci. 30 (2020) 44–65

Research Article

# Deuteron Plasmas Driven to Neutrality and $^4$He

Roger Sherman Stringham*

*Firstgate, 4124 Kapuna Rd., Kauai, HI, 96754, USA*

**Abstract**

This paper discusses Radio Frequency (RF) applied to cavitating $D_2O$, resulting in jet plasma implantation of charged separated electrons and a deuteron-compressed plasma pulse; these interactions involved hot charged particles at an effective temperature of $10^4$ K in a sub-picosecond time frame A. Free electrons were focused on clustered deuterons that compressed the deuterons like a spherical piston, squeezing a Meso-Cluster (MC) of deuterons. The compressed clusters were different from the deuterium clusters used by A. Takahashi. A reaction pathway similar to muon fusion was observed. The RF applied at a deuteron resonance, produced charge neutrality in the plasma's electromagnetic (EM) pathway where alpha production was observed. Each MC consisted of 2–100 deuterons. Here we will use 10 deuterons to describe the MC and its alpha production, within time frame A. The changing MC density, pressure, and temperature were critical to alpha production, within time frame A. The MC volume was about $10^{-39}$ $m^3$ and compression force was continuously applied to the MC located at the target foil (TF) surface. The heat transport was fast, and MCs were confined by electromagnetic fields (EM) tangent to the MC interface and motion of the neutralizing electrons. It is conjectured in this paper that the neutralizing plasma in time frame A produced a shockwave (SW) using a single electron to form a D atom that fused two deuterons in the MC to create an alpha. Before the fusion reaction, the surface target foil atoms were cavitating for an active period of 100 ns duration with each RF cavitation resonance cycle (see the main text in Fig 4). The physical basis for the conjectured deuteron fusion reaction consisted of a preliminary compression cycle due to the electromagnetic field applied to the deuteron MC for a few hundred femtoseconds, followed by a rapid expansion. The compression cycle produced an effective temperature sufficient to create an alpha particle from the compression of two deuterons. The expansion cycle produced a slight temperature drop, allowing a deuterium ion to recombine with a low energy electron. This produced an orbital electron capture in the MC, forming a deuterium atom that jumped a distance 60,000 times larger than the deuteron's ionic radius. It is conjectured that this impulse fused two deuterons in the MC into an alpha particle. The Mass Spectrometer (MS) measurements of collected gas samples produced by RF MHz cavitation in Ar-saturated $H_2O$ or $D_2O$ in a target foil lattice supported this conjecture. This conjecture was only a model, as other reaction pathways likely exist. Malcolm Fowler of McFarland Instrumentation Service (AIM) performed the MS analysis for He4 in the gas-phase RF reaction products. The analysis for tritium was done by Tom Claytor of High Mesa Tech (HMT). Pd TF were checked for any $^4$He retained in the Pd lattice. Electron mobility and target foil crystal types (face centered or body centered) may play an important role in the location of $^4$He in the lattice structure.
 ISSN 2227-3123

*Keywords:* Cavitation resonance, Deuterons, Free electrons, MC clustered radio frequency, Target foils, Time frame

*E-mail: Firstgate@earthlink.net.

© 2020 ISCMNS. All rights reserved. ISSN 2227-3123

## 1. Introduction

The author discovered archived target foils that had been run in 1994 at Los Alamos National Laboratory by applying 2 MHz of RF to the foils in argon-saturated deuterium oxide. The 1994 target foils were re-analyzed recently by a high sensitivity mass spectrometer (MS) for the presence of $^4$He and compared to the old data reported previously [1]. The collected gas samples were contaminated but the target foils were not. This data was recovered from old 1994 files and showed a reaction pathway that involved the implantation of electrons and deuterons into the Meso-Custer (MC). It is commonly known that $^4$He remains stable in the metal lattice of the target foils; recent sensitive mass spectrometer measurements reported $40 \times 10^{12} \pm 1$ $^4$He atoms in the target foils from 1994. The background $^4$He in the argon tank that was used in all experiments was measured at $0.200 \pm 0.006$ ppm.

The current gas samples were collected and measured with the assistance of Tom Claytor for tritium and Malcolm Fowler for $^4$He. The new MS was sensitive to 0.1 ppm. A chemically assisted reaction pathway to nuclear products appears to be possible and reproducible. New $^4$He data produced by several RF experiments in the megahertz range is introduced in this paper. The D+D $\rightarrow ^4$He reaction mechanism remains valid for the new gas phase studies by Malcolm Fowler, based on mass spectrometer data from collected gas-phase Ar/$D_2O$ samples.

The current tentative measurements from the gas phase of RF experiments with Pd target foils show amounts of $^4$He that are consistent with the 1994 measurements. The reaction mechanism appears to be the same, as suggested by the measured presence of $D_2$ and DOOD in the evolved gas [2]. This $^4$He was found in the Ar gas phase of the RF reactor with the difference being a contribution from the Acrylic surface of the RF reactor and its ions measured in the RF reactor's Ar gas phase. In summary, the old data and new data suggest the same reaction mechanism is present in both data sets, supported by the mass spectrographic measurements of steady state $D_2$ and DOOD. The mass ratio of $D_2$ and DOOD was consistently found in all samples over the last 27 years and is an important marker, as the same ratio appears in isolated systems impervious to time and instrumentation.

## 2. Cavitation Measurements

The goal of cavitation is to produce an MC by compression of deuterons and implant them into a metal lattice, typically palladium. As shown in Fig 1, when RF between 0.02 and 2 MHz is applied to deuterium oxide saturated with argon, many bubbles are produced. Only a select few bubbles will be resonant and assist in the formation of MC. Those that are of the resonant size, will follow the red trace in Fig 1, rapidly increasing in size, followed by a rapid and violent adiabatic collapse of the resonant bubble. At this point, the resonant/dense bubble ruptures to produce observable sonoluminescence (SL) and forms a compressing jet plasma that implants electrons followed by deuterons into a nearby target foil (TF). $^4$He is produced in the MC during the time frame A, as depicted in Fig 1. When the resonant (dense) bubble collapses, it is conjectured that the effective temperature reaches $10^4$ K or higher, which is sufficient to produce $^4$He from two deuterons. When the bubble collapses, the effective temperature declines slightly and allows the recombination of one deuteron with an electron, producing a recombination SW capable of igniting single or multiple alpha fusion events within time frame A.

It is of note that at higher RF frequencies, the craters observed on the surfaces of typical target foils are of a similar size (50 nm diameter). The amount of energy required to create the crater can be estimated by estimating the volume of the missing metal, or ejecta. The number of lattices in the ejecta can be estimated and the energy required to rupture a single lattice of the target foil can also be estimated ($\sim$21 eV). With this data, the implied energy released in the target foil can be computed and is typically $4 \times 10^{-12}$ J or 25 MeV. This value is consistent with the D+D $\rightarrow ^4$He reaction pathway.

The RF system is different from often-studied resonant systems [3] in that cavitation power is input into the RF reactor producing 40 W at about 1.3 atm of Ar-saturated $D_2O$. Typically, SL is coupled to the RF oscillating power input, as energy from the collapsed bubble is focused on producing a continuously pulsing SL emission. This energy

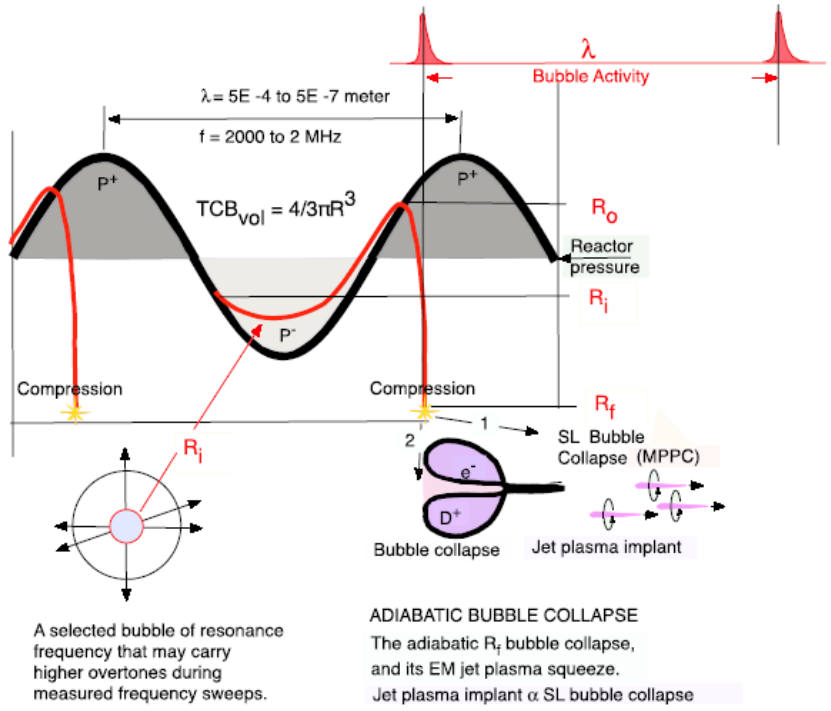


**Figure 1.** Acoustic input into water near a target foil, will resonate together to induce both observable and microscopic damage to surface and volume lattice of the TF. This damage can be catastrophic to the TF lattice depending on the power, frequency, and time [3]. The violent collapse of the bubble is less destructive as the frequency increases, as the bubble is reduced in size. The path of bubbles is shown in red, and its activity spread is shown also in red (see Fig. 3). During one cycle the measured SL emission is coupled to the jet plasma. The top arrow shows the extent of frequencies studied.

is dissipated in the lattice structure of the target foil (TF). The SL emission is monitored by a Multi-Pixel Photon Counter (MPPC) from Hamamatsu; the multi pixel devices show the system is in active mode about 10% of the time. The rest of the cycle time is spent in recovery mode for the next 10% active duty cycle. The active pulse, shown in red, is coupled to the general wave cycle. The system described above produces powerful acoustic output, and is focused on implantation of energy into the MC. The initial bubble, with radius $R_i$, begins in the negative pressure zone (P-negative) and gains momentum, reaching a maximum with bubble size, $R_o$; the bubble experiences a momentum-overshoot and is turned around in a recoil response, entering the high-pressure $P^+$ zone as a high velocity pulse with SL emission and a high-energy jet plasma, as indicated by the yellow stars shown in Fig 1. The SL is coupled to the electromagnetically squeezed jet plasma and is accelerated by the jet plasma, leading to energy dissipation in the TF.

### 2.1. Acoustic measurements and beats

A Polyvinylidene Fluoride (PVDF) sensor strip was used in conjunction with a wide band pick-up using channel 2 of the TDS784D oscilloscope; the scope output shows the beat from the presence of another close-by frequency input that is about the same frequency as RF amplified input. The presence of the two signals may become a useful parameter to manipulate experimentally.

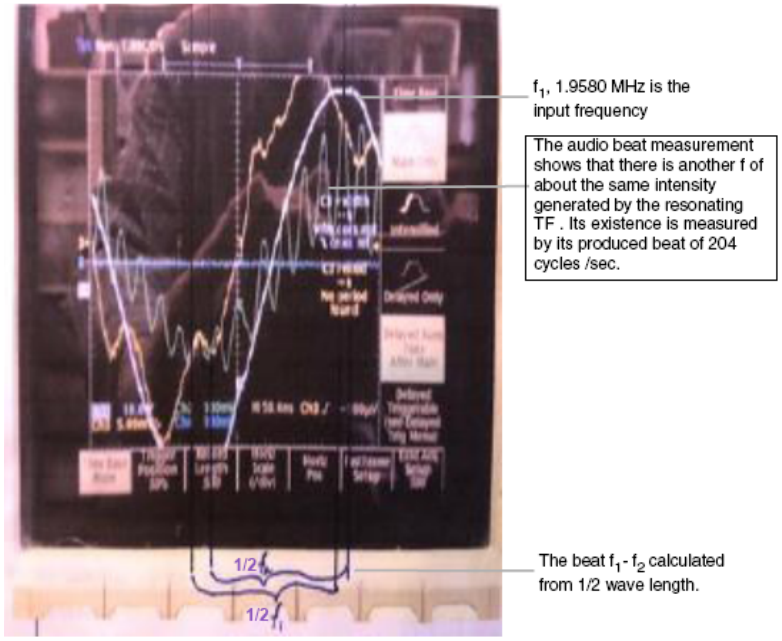


**Figure 2.** Shows a photo of the oscilloscope display during data collection in the RF running mode, with the RF input to the piezo antenna the half wave $(1/2f_1)$ depicted in white, and the audio output from the PVDF sensor $(1/2f_2)$ in green. The audio pick-up (green trace) represents the $f_2$ input frequency with a similar amplitude and the white trace $(f_1,)$ represents the RF generator input of the target foil resonance. The two signals of different frequencies alternate between constructive and destructive interference, producing a beat frequency $(f_b)$ that contains the alternating high and low maxima of the two interfering signals: $f_b = f_1 - f_2$. The MHz frequency of the RF input $(f_1)$ minus the TF frequency of the second signal $(f_2)$ is expected to be smaller than $f_1$ and is calculated as $f_1 - 204 = f_2$ cycles/s using the sums and differences equation. This calculation may be further complicated by the presence of overtones in $f_1$, as evidenced by the irregularities in the $f_1$ sine wave.

## 2.2. SL measurements

Figure 3 shows the MPPC SL output in ∼100 nm width SL emission pulses, shown in volts as blue peaks and they are coupled to the acoustic output (red trace); the scale is 1000 times the voltage output of the Hamamatsu MPPC. The scale is 50, 100, and 1600 pixels with wavelengths between 350 and 1000 nm. The reactor is a unique 1.5-inch diameter cylinder of machined polycarbonate, using a 0.0031-inch Pd wire as a TF and a cylindrical PZT piezo resonating at 0.63 MHz with Ar-saturated $D_2O$ circulating through it. The reactor produced about 40 data graphs similar to the one shown in Fig. 3. The center of SL emission from the cylindrical PZT piezo was from the two 5 mm end openings, which made for a rather large emission source for the SL (9 mm). The SL measurements were taken in a 36× 36× 36 $cm^3$ dark box at three different MPPC distances within the box, using three different Hamamatsu MPPC devices while measuring their voltage output. The SL emission is proportional to the number of jet plasmas produced before implantation into the target foil wire lattice (see Fig. 1). The SL measuring emission surface has a spherical radius of d, and the largest sensing spherical surface area was 16 cm from the source (8 and 16 cm radius). The matrix of the time vs volts (4000 × 300) was adjusted a few nanoseconds to bring the voltage data into focus, showing the 100 ns periods on cavitation activity (blue).

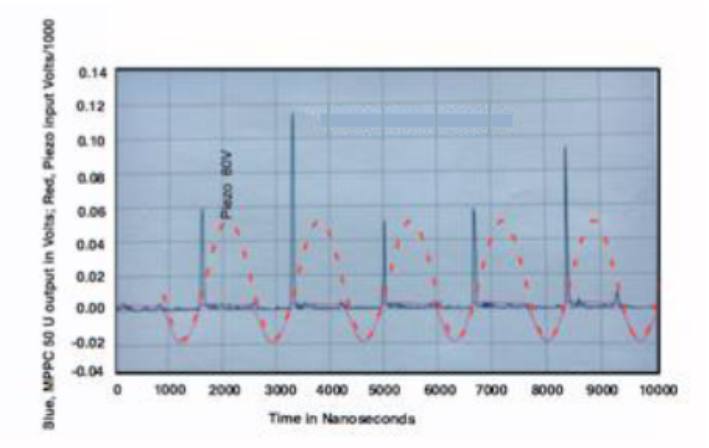


**Figure 3.** It is a typical data sheet from a reactor that circulated water through a cylindrical PZT piezo 17 mm long, 11 mm OD and 5 mm ID. This was done in a sealed light box, where SL emission was measured by MPPC devices donated by Hamamatsu. Through the center of the piezo is a sealed Pd wire; the acoustic energy was focused at the wire surface, as depicted by the red trace. The SL detection MPPC device was stimulated by a DC 80 V bias input. The SL output, depicted by the blue trace, was measured as a 100 nm half width voltage peak. The velocity of sound through $D_2O$ was 1600 m/s, the distance from the inside diameter to the wire was 2 mm. The frequency was 1600 m/s over the distance of 2 cm resulting in 0.8 MHz frequency and the blue trace represented 100 nm of active resonance time.

The MPPC output is scaled to the number of photons counted times the proportional area of

$$\frac{\text{measuring sphere surface area}}{\text{MPPC detecting surface aera}}.$$

The bubble population that is involved in the sonofusion is applied to the surface of the oscillating TF wire and the piezo. It appears that the increase in the MHz range frequency that utilizes a much smaller bubble size maintains the same energetics and produces $^4$He, while operating on a 10% duty cycle in the active mode as shown in Fig. 3 (also see $\lambda$ in Fig. 1). It was found experimentally that operating at 20 kHz produced significant damage to the target foils, while operating at 2 MHz [4] produced less damage to the foils and motivated operating at higher frequencies.

When SL emission measurements are positive in the reactor and coupled to the input frequency, shown in Fig. 3 in red, plasma events like dissociation and recombination are occurring. The bubbles issued from both the piezo and the TF surfaces are involved in producing a deuterium ion and electron plasma for implantation in the MC [4]. The SL measurement shows the system is operating in a zone that is producing implanted MCs in the TF, and the implantation rate is proportional to the measured SL intensity as the two-bubble collapse products of SL and jet plasma, are found in every mass spectrometer study. There is also confirmation of SL products and jet plasma from recent mass spectroscopic work done by Malcolm Fowler of $D_2$ and DOOD steady state measurements [2].

### 2.3. System overview

Examining in more depth the relationships that makes MC implantation work, note that the SL emission for one cycle is proportional to the number of plasma jets that are shown in connection with a single SL pulse in Fig. 1. A collection of SL signals that show a sum of SL events are pulsed along a time line for 10,000 ns, as shown in Fig. 3. For one MC pulse starting in the gas phase in time frame A at $\sim$10,000 K, where $D_2^+ \rightarrow 2D^+ + e$ and the implanted jet plasma pulse are in a state of free mobile electrons; the free highly mobile electrons surround the almost stationary MC deuterons

and atoms of the TF lattice. The system is naturally driven by the neutralization resulting from the charge difference between the spherical electrostatically focused mobile electrons at the center of the immobile MC. There was seldom a $D^+ + e^- \rightarrow D$ recombination because of the high temperature. The time frame A and the mobility of the particles that make up the MC in the gas phase produced a total of approximately $10^{12}$ MC implantations per-second, producing approximately 40 W of anomalous power. Each MC is an active implant center; at each MC site, the deuterons within the MC are electrostatically squeezed with the center focus of the spherical cloud mobile free electrons, and this squeeze produces compression heating of MC deuterons. Additionally, an electromagnetic tangent field provides the surrounding containment of TF atoms that also squeezes the deuterons but does not promote recombination in the MC. The measured amount of $^4$He is unexpected but is a result of an inefficient process.

The ultimate goal is to make this a more efficient process. In the given time frame A, the free electron mobility, points to a periodicity shadow in the unit cell that is occupied by an MC; during its TF confinement, the mobility drift of the target foil's relatively large atoms during MC containment is small. A deuteron cluster in the atom's unit cell interstitial space has a higher mass density than the target foil resulting in a static MC in time frame A. Basically, there is no real movement of atoms except the compression-producing electrons during the MC deuteron confinement. In the gas phase, the target foil lattice atoms remain in the same lattice space, exhibiting their shadow behavior in the gas phase during the time frame A. In reality, there are continuous changes of crystal structure during the heat-pulse compression, and structures such as BCC and FCC crystals are not clearcut on the atomic scale [4]. The activity of crystal changes has time factors for changes along with Brillioun effects [5].

## 3. Experimental

### 3.1. The RF reactor

The radio frequency system is a non-obvious extension of SF, where a replacement of the oscillator with an RF input to the 1.7 MHz piezo is now an antenna that is tuned to minimum RF reflection and maximum admittance with a standing wave ratio (SWR) of one, indicating 100% signal transmission. There are other tuning methods that can be utilized: oscilloscope voltage, the frequency resonance, the visual $D_2O$ surface, and the oscilloscope overtones. Some new discoveries about the cavitating system have been made during this experimental campaign: (1) there is more than one vibrating surface and (2) the fundamental vibration may make some large contributions to the resonant bubble population via overtones.

Experimentally, RF interference was a major concern that accompanied all measurements made while the RF system was running. To minimize RF interference upon instrumentation, a duty cycle was introduced of 30 s on and 5 s off that provided an adequate time window for credible measurements of temperature; this feature was built into the calorimetry of both the RF mode and calibration mode (see Figs. 5–10).

Two years of RF practice runs with $H_2O$ suggested that enough knowledge was in place to do controlled runs with $D_2O$. There was a completely different philosophy in the new RF rector. The reactor was no longer a small polycarbonate 50 g reactor with a 1 $cm^3$ of actively cavitating volume with 1 ml circulation rate of $D_2O$.

The new RF reactor was machined by Hans Huber from a 6-inch acrylic tube, having a 2-inch diameter with quarter-inch walls. A one-inch thick by 3-inch diameter disk top was provided, where all the utility and measuring pass-throughs were positioned, except for the RF input placed at the tube bottom with the RVDF audio pickup (see Fig. 4A). A 1/8-inch diameter copper cooling coil of 16 turns was submerged in the static $D_2O$. This coil moved fluid at a measured rate of $1\pm$ 0.02 ml/s (see Fig. 4B). The purpose was to remove heat, keeping the $D_2O$ at a constant temperature that was reached after running about 1000 s. The water coolant flows from Cu coil # 1 through a closed loop to an equivalent second copper coil submerged in 3.5-liter coolant reservoir and circulates back to the $D_2O$ coil #1 for another cooling cycle (see Fig. 4B). The pump is an FMI displacement pump moving $H_2O$ coolant measured at a constant ml /s. The reactor measured heat $DT_1$ (the output of the coil minus the input of the coil) plus $DT_2$ heat

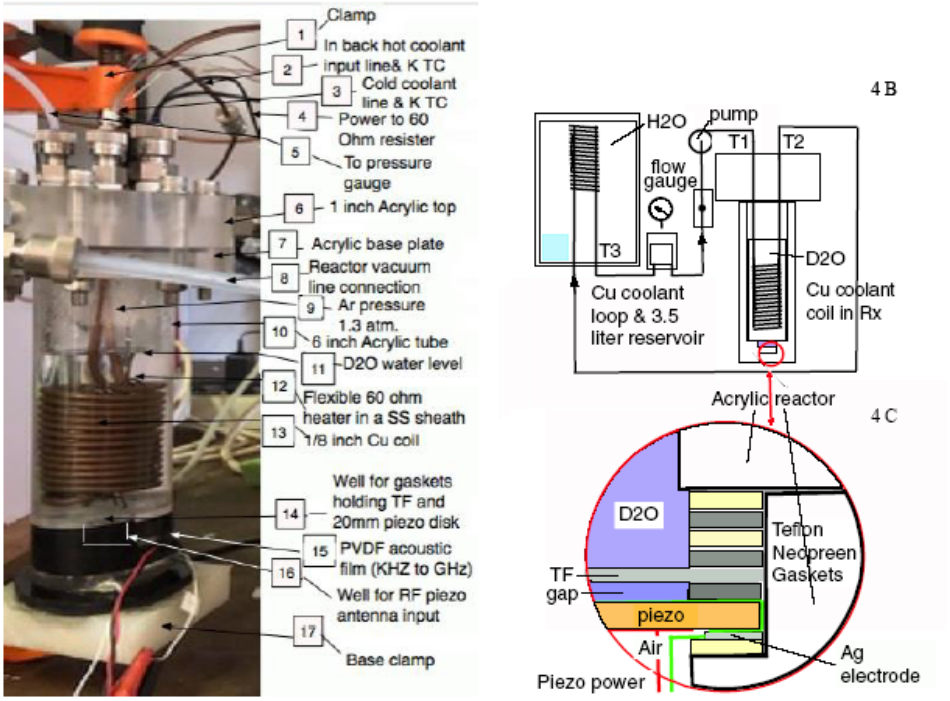


**Figure 4.** (A) The acrylic RF reactor is compressed to seal the Ar-saturated $D_2O$. The bolted top plate, 6, holds all the connections. The heat removal Cu coil is completely covered by 80 g of $D_2O$, Fig. 4B. The 60 Ω resistance heater from ARI was completely submerged, 11. The gas phase Ar, 9, with a trace of $D_2O$ was present at its vapor pressure at a total pressure of 1.5 atm. The 20 mm piezo disk, RF piezo, is centered in the bottom with the target foil, approximately 1 mm above in the cavitating $D_2O$. (B) The coolant loop between the reactor and 3.5 l coolant reservoir maintains the steady state temperature during the power inputs to the RF and calibration modes. Note the flow control was by the FMI displacement volume pump at ∼1 ml/s. (C) The red circle shows a corner of the acrylic reactor in light blue; the placement and sealing of the TF, 5×18×0.01 $mm^3$, and piezo shows the 1 mm gap. Bubbles are formed in the gap and the top and bottom of the TF surface $f_1$ and $f_2$ surfaces of the target foil (see Fig. 2). The piezo ground Ag ring with green lead and the positive input is red bottom service for the 1.6 MHz PZT 20 mm disk piezo. The Teflon and Neoprene gaskets are spacers and seal for the piezo and TF.

removed to the 3.5-liter coolant water cooled by Cu coil #2. The sum of these two DTs is the total heat produced by the running reactor.

### 3.2. Experimental set-up

The RF system gathered data using a video camera correlating the many parameters, using the sweep second of the clock, #14, to point out and store any running changes during an experimental process. The geometry of the RF run from the 50-g polycarbonate circulating $D_2O$ liquid system uses a 5 ×1.5-inch column of $D_2O$ while keeping the static $D_2O$ close to steady-state temperature by using a 16 loop Cu coil. The coil is 1/8-inch OD and about 2 inches long submerged in the $D_2O$. The setup required about 1000 s to reach steady state.

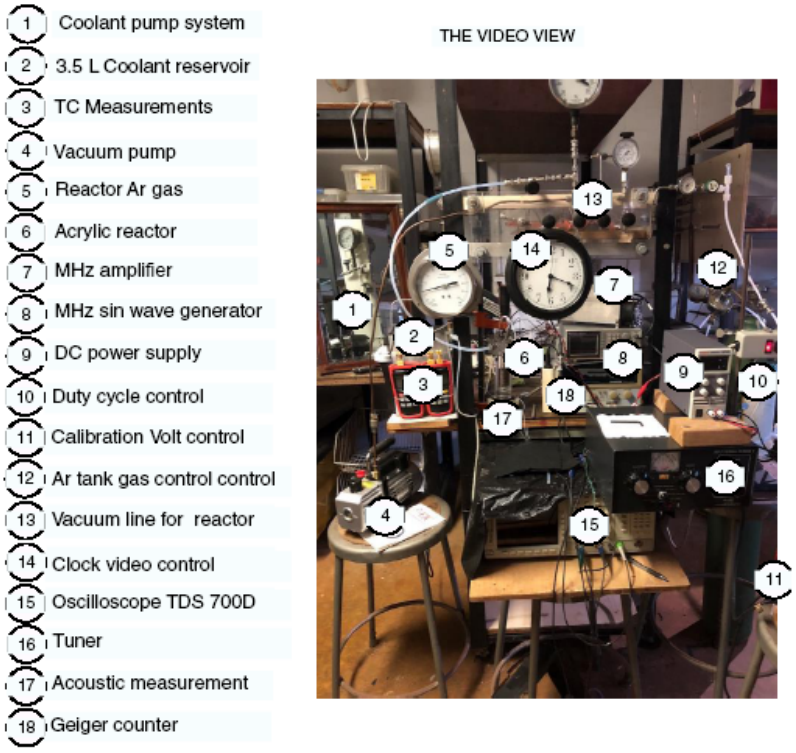


**Figure 5.** The video screen is set in the plane of the clock #14 to cover as many parameters as practical. The Cu coils #6 and #2 form a loop moving heat from #6 to #2 (see Fig. 4B). The coolant circulation that is exempt from the duty cycle flows at a measured rate of about 1 ml/s (#1). The RF input signal is provided by an Eventek 3010D audio-amplifier (#8). The HD communications HD30866 RF amplifier and its DC power supply are shown as items 7 and 9, respectively. The oscilloscope #15 and tuner #16 monitor the RF signals. The vacuum gas system involves the vacuum pump #4, vacuum line #13 and the Ar tank #12. PVDF sensor film #17 detects the complex beat signal in the MHz range indicating the presence of two signals with approximately equal RF intensity.

### 3.3. Example of collected data from RF run RF4 $D_2O$ and Pd

**Explanation of Fig. 6**

Moving Reactor heat from the reactor to the 3500 ml water coolant reservoir reducing the running temperature. The heat measured via T2 - T1 90 (Cu oil in and out) for both run and cal. mode. The cal. mode substitutes a 60 Ω, 10 W heater input for the RF input. coolant water flow rate is measured is for the combination One and Two reactor inputs for the Cal. Mode. The total watts input comes from the resistance heater, $V_2/R = 202/606.7$ W. One, at measurer the output coolant flow 1.08 ± 0.02 ml/s. There is a continuous heat loss to the coolant keeping the running low as possible (good for the cavitation process). The power input from a 20 V Variac is 6.7 W. The key is the power loss to the 3.5 l coolant heat gained at a steady state temp of 3.2°C. The rate of heat loss operating at low DT. The total heat is 6.7 and provides a scaling factor for the run mode. The 6.7 W produces 3.2°C. For the RF input it has the same temperature drive for the same 87 g of $D_2O$. An Attempt was made to make the two modes and running during cal. modes. The 6.7 W input and temperature for the cal. mode is the scaling-factor for watt calculations: Run, Cal.

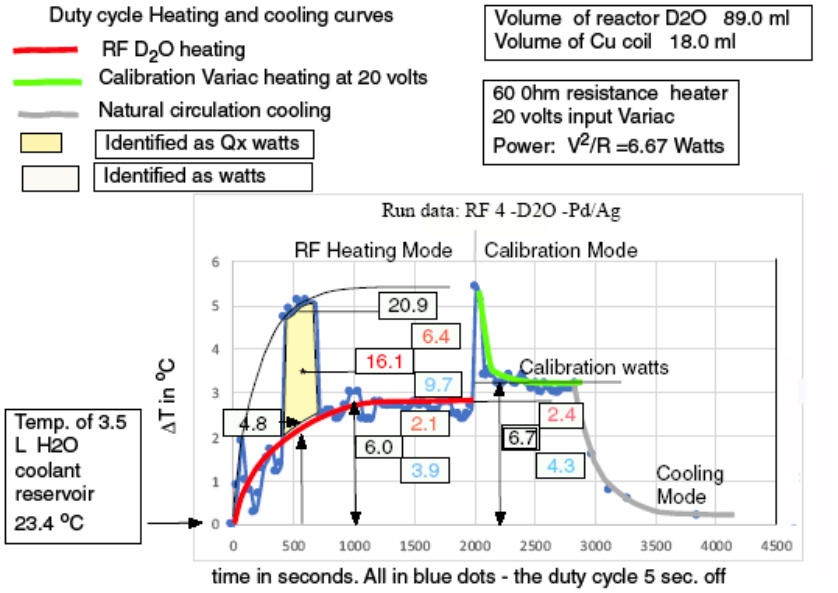


**Figure 6.** See the Explanation of Fig. 6 below Section 3.3

and Qx modes shown in Fig. 4. Run RF #4 $D_2$ and Ag. The RF data, blue dots, are are reduced to numbers, and are keyed to the calibration mode resistant heater Watts input. Volts$^2/\Omega$ = 6.7 W during the duty cycle. This value scales with temperature °C.

### 3.4. Typical RF mass spectral analysis

Run # RF 4 $D_2O$ and Pd. Data collected Apr. 30, 2018 and shown below the MS RAS $^4$He analysis by Malcolm Fowler, in Fig. 7. His MS measurement was 0.363 ppm in $D_2O$

### 3.5. RF EDX data

EDX of RF cavitation TF surface.

## 4. The Meso-cluster

### 4.1. A possible model

When trying to explain the RF process presented in Fig. 9 as a single event, one consideration is to think of the MC as a group of deuterons acting as a single unit in time frame A. The MC can be thought of as a small collection of charged bosons under compression at a high temperature. The deuteron density increased due to compression and due to the neutralization process ($D^+ + e \rightarrow D$) within the hot plasma of the MC. The instantaneous charge communication kept the neutralization process from occurring at the end of the neutralization drive of the plasma when the temperature dropped near the end of time line A. The point of a single recombination of the D atom produced a corresponding SW

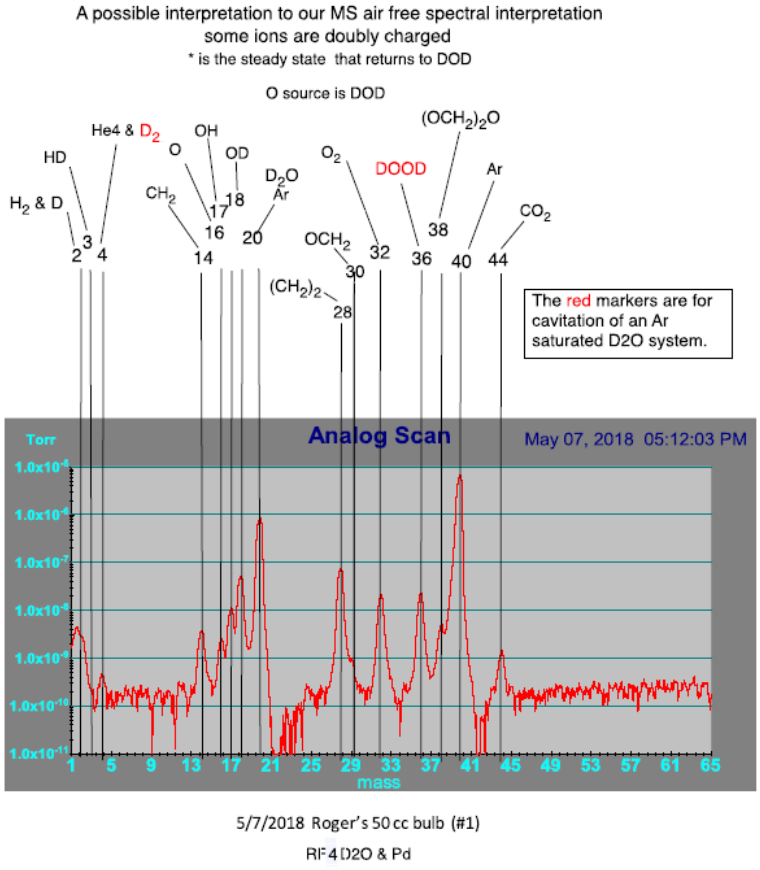


**Figure 7.** From [2] "Chemical species generated under ultrasound irradiation are attributed to the acoustic cavitation phenomenon". Under Ar bubbling, the species detected during the sonication of pure water are $H_2$ and $H_2O_2$ in agreement with the following equations transposed from H to D: $D_2O \rightarrow H + OD^{\circ}; D + D \rightarrow D_2; DO^{\circ} + {}^{\circ}OD \rightarrow D_2O$.

that stimulated alpha formation in the MC that had been neutralized with one cooled electron. One alpha was produced in time frame A, during the charge separation and neutralization process at the expense of one MC.

The above paragraph describes the timeline A shown in Fig. 9; the evolution of the MC is governed by the implantation of squeezed electrons and deuterons. Charged particles are driven toward charge neutrality in the MC plasma. The plasma remains below the critical density required to trigger the D atom shock wave (SW); this delay produces high compression temperatures due to the collapsed bubble cavitation jet resulting in squeezed and focused spherical compression of the deuterons forming the MC (Fig. 10B). The free mobile electrons implant first, followed by the less mobile deuterons to form the charged-separated MC plasma. Compression heating also occurs in the confining target foil lattice atoms by adding free ionized electrons that increase compression. The surface-implanted electrons are initially separated from the implanted deuterons in time frame A; the deuterons are electrostatically compressed in the squeezed MC plasma via its spherical piston action at the TF surface for ambient face-centered structure, and in the TF volume for ambient body-centered structure.

EDX of RF cavitation TF surface

| | | GRAPH 1 | GRAPH 2 | GRAPH 3 |
|---|---|---|---|---|
| Atoms identified Num. | Type | H2O RF3 Pd | D2O RF4 Pd | Piezo RF 2 Pd |
| 8 | O | 80.0 | 59.0 | 23.10 |
| 46 | Pd | 7.9 | 22.9 | --- |
| 14 | Si | 4.9 | 15.3 | 9.14 |
| 13 | Al | 2.6 | 0.5 | ---- |
| 29 | Cu | 1.04 | 1.01 | 6.34 |
| 28 | Ni | 0.97 | 0.69 | 42.9 |
| 12 | Mg | 1.77 | 0.00 | ---- |
| 26 | Fe | 0.58 | 0.75 | ---- |
| 16 | Su | 0.11 | 0.61 | ---- |
| 40 | Zr | 0.00 | 0.40 | ---- |
| 15 | P | | | 0.71 |
| 22 | Ti | | | 3.55 |
| 6 | C | | | 2.97 |
| 11 | Na | | | 0.83 |
| 7 | N | | | 0.12 |
| | | ~100% | ~100% | ~100% |

**Figure 8.** Shows there were a lot of surface oxides, and the irradiated target foil surfaces showed the unique presence of the $^{24}$Mg isotope in graph 1 of Fig. 8 from this series of EDX measurements. The reaction pathway to such a transmutation is obscure, but a pathway that utilizes $^{16}$O, where 2O $\rightarrow{}^{24}$Mg $+{}^{8}$B and $^{8}$B $\rightarrow{}^{4}$He + alpha + $\beta^{+}$ $^{8}$B has a half life of 770 ms [6]. The isotope $^{24}$Mg is unique in the EDX graph 1 of Fig. 8 and $^{16}$O at 80% concentration in a proposed pathway to account for its EDX presence in a cavitating Ar-saturated $D_2O$ fluid with implantation of plasma jets into a Pd foil. Graph 3 of Fig. 8 shows there is no Mg contribution from the piezo. Both the $D_2O$ and $H_2O$ EDX graphs had target foils of Pd that were cut from the same 0.1 mm stock from Ithaca. The volatility of a Mn complex is coupled with 12 mass-ratio in RGS mass spectroscopy of RF 3 $H_2O$ and Pd collected products.

The plasma temperature at ∼10,000 K allows for charge neutralization, but no recombination to D atoms [11]. The collection of 2–20 squeezed deuterons form the MC. At the lower frequency of 20 kHz the MC population will be larger [3]. Under these conditions, the deuterons have a radius of ∼1 fm. The early-stage compression diameter of the MC is on the order of 1000–100 fm. As the compression progresses, the mobile electrons move into the MC, neutralizing its plasma charge; however, the elevated temperature prevents recombination to form neutral deuterium atoms.

Statistically, near the end of the compression cycle, the density increases and temperature decreases; under those conditions, the probability for a D-atom recombination in the MC increases. A single D-atom formation expands $10^9$ times in volume in a femtosecond, initiating a local SW impulse in the MC space. This rapid space expansion impulse in the MC produces one or more alphas, and no detectable radiation. The impulse time is very fast making for a powerful local energy density impulse, which destroys the MC, produces alphas, heat, voids and micro TF spheres in the target foil lattice [12]. A single alpha-producing event requires $3.83 \times 10^{-12}$ J (24 MeV), and this energy release is consistent with the energy required to form the observed single event ejecta sites. Numerous examples of single-event ejecta sites are found in SEM photos of target foils with face centered cubic crystal structure. Target foils with body centered cubic crystal structure do not exhibit the single-event ejecta sites (unit crystal lattice).

Evidence of alphas was found in several target foils where surface alphas were ejected at the surface of the target foil and are associated with surface craters and micro-spheres, as documented using scanning electron microscope photography (single events). The presence of crater ejecta was always associated with $^4$He in the collected gas samples of argon-saturated $D_2O$ measurements. When the data was examined for surface craters in BCC Ti target foils, none

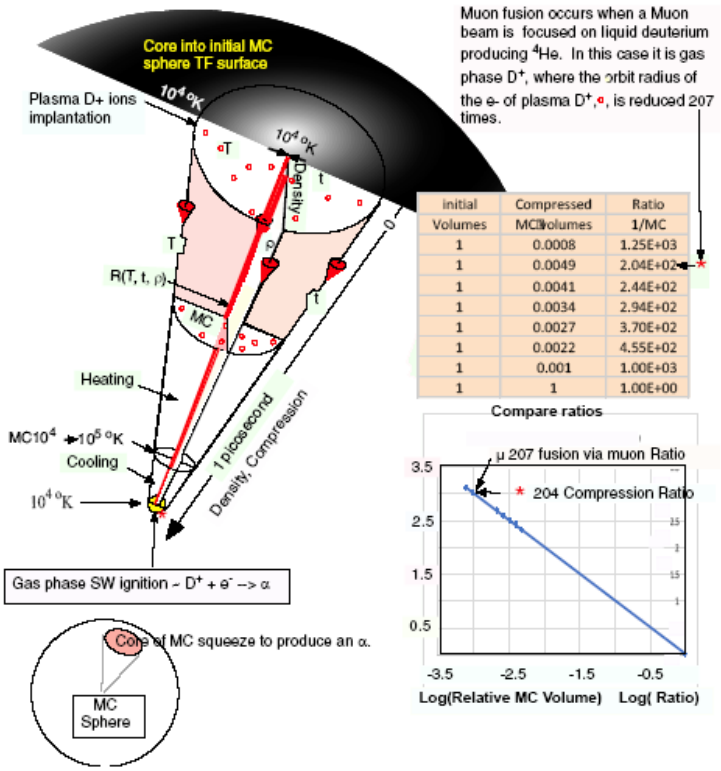


| initial Volumes | Compressed MC Volumes | Ratio 1/MC |
|---|---|---|
| 1 | 0.0008 | 1.25E+03 |
| 1 | 0.0049 | 2.04E+02 |
| 1 | 0.0041 | 2.44E+02 |
| 1 | 0.0034 | 2.94E+02 |
| 1 | 0.0027 | 3.70E+02 |
| 1 | 0.0022 | 4.55E+02 |
| 1 | 0.001 | 1.00E+03 |
| 1 | 1 | 1.00E+00 |

**Figure 9.** The figure shows the reaction sequence following the ($D^+ + e$) plasma implantation, comparing MC fusion to muon fusion [1]. The black sphere is the MC at $T$ on the time line A. A core from the MC is visually expanded to reveal the stages during the time line A. Electromagnetic compression and the magnetic target foil containment of the MC contents initiate the pathway to $^4$He production. Three important parameters, temperature, time, and density are aligned with the red core MC compression in the implanted TF lattice. Note in Fig. 9 that as time advances, the contents of the MC are brought closer together by compression; this action and the two graphs show the similarities to muon fusion, which in this case occurs at an effective temperature of 10,000 K. The compression of deuterons conjectured here occurs much faster than muon fusion [7] (see Fig. 3); the fusion conjectured here occurs at a much higher temperature using an SW in the MC plasma ($D^+ + e \rightarrow D$). The impulse energy is derived from the shockwave's destruction of the MC in the blue cooling zone with D atom recombination, producing an alpha event and $^4$He (also see Fig. 13).

was observed. Mass spectrometry shows that $^4$He is trapped in the active Ti TF lattice volume. This was concluded when 3.83 $\times 10^{+12}$ $^4$He atoms above measured background levels were released from a vaporized sample of Ti TF [1].

So, there is a dilemma. Reactive face centered cubic (FCC) target foils produce $^4$He with numerous single-event ejection sites at the TF surface; by contrast, body centered cubic (BCC) target foils trap $^4$He somewhere in the lattice. The evidence shows that alpha activity in the FCC target foil is expressed by alpha ejection at high temperature, while alpha activity in BCC target foils is trapped within the host metal. The FCC unit crystal has twice the number of atoms as the BCC. Why is there a difference between FCC and BCC target foil activity?

There have been fragile 1 $\mu$m diameter hollow tubes observed in SEM photos [8–10], and much evidence from other sources. These tubes are fragile and not expected to last more than a fraction of a second. There is a critical

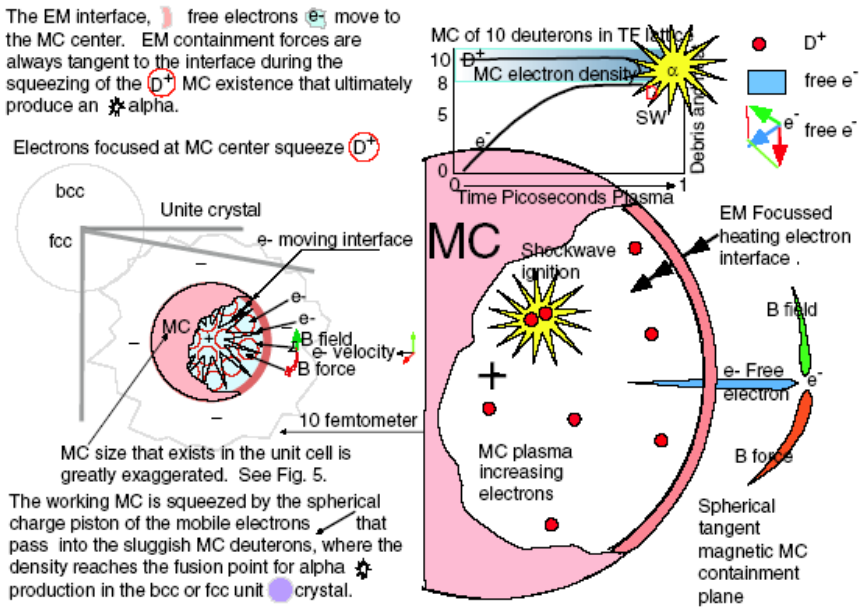


Figure 10a Figure 10b

**Figure 10.** (a) Shows the possible connection of the unit cell to the MC The gray lines indicate the placement of the MC in the unit cell in time frame A. The purple sphere is the corner of a BCC or FCC unit cell. Of the many different target foils tested, the only BCC lattice crystal measured was the hot surfaced titanium target foil. All titanium foils tested had $TiO_2$ microtube surface layers of iridescent color consistent with a surface standing wave. The measured titanium target foil, Ti-3A, produced $^4$He that was located in the interior lattice structure of the titanium foil. By contrast, The FCC target foils showed a substantial number of single- event surface craters that are perhaps equivalent to the energy of one alpha event and will be treated that way in the text that follows (ICCF 20). Therefore, the $^4$He measured from titanium target foils not showing ejecta sites was not consistent with two Palladium samples that showed many ejecta sites, but no lattice $^4$He. (b) Shows the detail of the MC and its surrounding free electrons; the light blue sphere to the right is focused at the center of the MC sphere. The graph at the top shows the penetration of electrons that neutralize the plasma but are too hot to recombine [13]. The movement of electrons, by way of the electromagnetic force, compresses the MC contents. Momentum carries into the cooling mode of spherical charge as the electrons move to the center of the MC, where a D atom forms, creating an impulse SW capable of producing heat and $^4$He.

difference between the BCC and FCC target foils, based on properties of the unit cell [13] or differences based on other factors yet to be considered.

### 4.2. Summary of the activity within the MC

Figures 10a and b depict the MC activity in time frame A (less than a picosecond) from the point of view of the MC itself. In the model, the MC is a cluster of deuterons that have an affinity and repulsion for each other, being hot bosons surrounded by mobile elections in a charged-separated plasma containing only deuterium ions [14]. The radius of a $D^+$ is just over a fermion and the electromagnetically compressed MC will locate somewhere interstitially in the unit crystal (see Figs. 10A and 11B). The unit cell for the FCC contains four atoms, the BCC unit cell contains two atoms and is one-half as large as the FCC unit cell. The MCs can locate anywhere in the host metal lattice. They are sufficiently small so that all components are only slightly larger than one fermion.

Figure 10a shows the corner of a unit cell and the MC dimension that shows a free electron pushing concentrically inward to a focus point while the mobile electron generates a magnetic field with force tangent to the interface. The electrons are the only particles moving in time frame A. Figure 10b depicts the conjecture that the deuterons contained in the MC can be compressed by forces that include the force of an orbiting electron. It is also conjectured that the chemical energy (15.5 eV) released during atom–electron recombination is sufficient to produce D+D $\rightarrow$ $^4$He + 24 MeV because of the high particle density within the MC. The proposed ignition energy comes from $D^+ + e \rightarrow D +$ 15.5 eV, producing an effective high energy shock wave pulse that forces at least two deuterons in the MC to fuse.

### 4.3. The drive to neutrality

For discussion purposes, assume the MC contains 10 deuterium ions and no neutral deuterium atoms at a high temperature with electrons moving through the interface without recombination during the time frame A. The MC volume remains small, with its cluster of ten deuterons as an example. As the MC cools at the end of its compression cycle, a recombination occurs resulting in a shock wave with sufficient impulse energy to produce the $D^+ + e \rightarrow D + 15.5$ eV chemical reaction. The mobile electrons have a temperature, a velocity, and a direction that keeps the MC compressed and heated. It is proposed that the initial out of balance charge distribution drives the increasing energy density toward that of a muon fusion environment and is driven by a natural electromagnetic compression. At high temperature, Faraday's law of induction forces a mix of electrons and deuterons to form a neutral plasma, without forming neutral deuterium atoms [15]. The temperature is high and the impulse time (see Fig. 13), is of short duration, so there is no recombination forming neutral deuterium atoms (marked in red in Fig. 10b). At the end of the MC cooling cycle, an increase in the probability of recombination occurs, destroying the MC. A SW impulse of high energy density produces $^4$He and heat. The electron energy, velocity, temperature, mobility, and time are in resonance to produce this single event (see Fig. 10b).

### 4.4. The cycling of MC and electron mobility

The TF crystal system in time frame A at high temperature was not mobile enough to alter the solid phase periodicity order. In time frame A, the unit cell structure of FCC and BCC location of atoms was still intact. Although there is a possible interchange of crystal structure FCC to BCC at an atomic level at 1200 K [13] the lattice phase does not change much. The MC should be considered as an interstitial addition to the target foil lattice (see Fig. 11b). Modification of the melted surface of the target foil will keep changing to a fine-grained surface lattice, with the grain boundaries taking up the debris, as it is cycled through a continuous heating and cooling process. This atomic scale cyclical process alters the surface of the target foil to an approximate depth of 100 $\mu$m; low frequency cavitation input produces more target foil damage than does high frequency cavitation input as evidenced by SEM photos [3]

The surface of the TF in a cavitation field is generally exposed to small energy pulses continuously heating and cooling several million atoms at any given time. Recrystallisation tries to follow the input frequency by decreasing the surface crystal size as the frequency increases. Cavitation bubbles decrease in size as the surface tension increases. As the energy of the system decreases, the energy density increases so smaller systems have a better chance at making alphas. The smaller implanting events of the MC containing only a few deuterium ions are at too high a temperature to react. When the deuteron temperature declines slightly, a deuterium ion and a single electron can recombine to produce a small but energy-dense shock wave and an alpha.

The electrons in a high temperature environment of non-recombining plasma of deuterons and free electrons are focused on the squeezed deuterons. These short-lived MC-implanted deuterons are further heated and squeezed by these moving electrons to produce a fusion event in time frame A. The plasma electrons are the only species with mobility and are focused on the MC-implanted deuterons. The MC system is driven by charge separation driven to

neutrality in a process similar to muon fusion. As the MC deuterons reach a density similar to that of muon fusion, alphas begin to appear in the lattice [7].

## 5. Discussion

### 5.1. The FCC and BCC differences

The unit cell of Ti contains two atoms with a coordination number 8, and FCC contains four atoms, with a coordination number of 12 for their cubical and reciprocal lattices. The coordination number is the number of atoms touching in the unit cell. The reciprocal lattice of the BCC is the actual lattice of the FCC and vice versa. The X-ray diffraction patterns of BCC crystals are the same as the actual FCC unit crystal atom lattice distribution. The symmetry lines from the center of Brillion zones and Wigner–Seitz unit cells define their symmetry points. The Brillion zone for FCC is BCC and the BCC is the FCC Brillion zone. The mobility of free electrons dominates the time frame A of the MC with gas-phase probability of zero for finding an electron orbital to form the D atom producing the SW (SW)of $2D^+ \rightarrow \alpha$.

The probability of finding an electron orbit in the MC is zero, and not until the temperature and density are favorable to recombination ($D^+ + e \rightarrow D$) will there be a recombination event to produce a SW impulse to create an alpha in the compressed MC.

In earlier experiments, $^4$He was measured in the Ti bulk lattice either retained near the surface or deep in the lattice, as opposed to palladium target foils which produced $^4$He in craters formed at the surface. It is more likely for helium to be near the surface of the target foil than in the bulk lattice. The titanium target foils had a $TiO_2$ surface layer and trapped $^4$He in the Ti lattice. The palladium target foils were different and showed no measurable $^4$He above background level in the metal but it was observed that $^4$He was ejected from the palladium at sites that originated in the near surface. It was found that the energy required to remove the volume of ejecta observed in a single site was about 24 MeV, which is consistent with the energy released for the D+D $\rightarrow ^4He^+$ 24 MeV reaction. These crater sites are about 50 nm in diameter and depth. The number of palladium lattices in the ejecta volume is calculable and the energy to disrupt a single palladium lattice is known to be about 21 eV. So, the ejecta volume observed in a single crater suggested a single nuclear reaction of approximately 24 MeV. These small events were seen in low frequency events with more damage in high resolution SEM [3]. The SEM photos with high frequency experiments show the relationship between ejecta volume and single alpha production. Palladium lattice atoms that are ejected from craters along with alphas have been shown in many SEM photos. Various sized craters have been observed with ejecta volumes corresponding to an implied energy release in the form of integer multiples of 24 MeV single energy events. Measurement of ejecta volume is then conjectured to be an indirect measurement of the $Q$ for the reaction that produces alphas in deuterated palladium. No gammas were found that could relate to one or more alpha events. These correlated ejecta events were observed for FCC crystal lattices of Pd, Ni, Cu, and Ag. This finding is in contrast to observations made in the titanium BCC crystal lattice. A titanium target foil sample was studied by Brian M. Oliver in 1994 that measured $40\times10^{+12}$ $^4$He atoms, trapped in the exposed titanium, as analyzed by mass spectroscopy at Pacific Northwest Laboratories. There was no evidence of ejecta damage revealed by the several SEM photos taken of the sample surface.

The jet plasma surface implantation into the titanium target foil where the titanium BCC surface is modified by the presence of $TiO_2$ may explain the difference between FCC and BCC with regard to crater formation. The titanium sample surfaces contain deep layers of multi-colored iridescent standing wave patterns of $TiO_2$, featuring micron diameter tubes [8]. These surface differences may explain why the FCC target foils produce alphas at the surface while the BCC target foils produce alphas in the metal volume. The deep layers of $TiO_2$ buildup on titanium target foils by $D_2O$ cavitation may influence the location of alpha production.

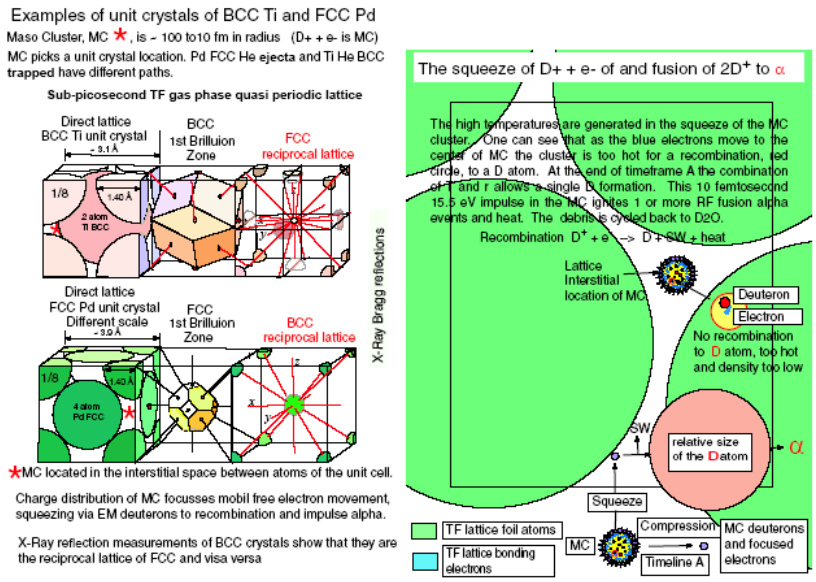


**Figure 11.** (a) Shows the periodicity of the TF lattice that for a sub-picosecond is stationary except for the mobile high temperature free electrons on the MC in the titanium BCC lattice or palladium FCC lattice. The compressed MC of deuterons is located in the interstitial space between atoms of the target foil. The red stars shown in (a) depict the spherical free electrons that compress the MC. The presence of many free electrons raises the temperature of the atoms contained in the TF lattice. Note that the unit cell of the BCC is the reciprocal lattice for the FCC lattice and vice versa, so the containment void space may have some important differences.

### 5.2. Unit crystals and MC deuterons

Figure 11b Shows that when the temperature remains high in the TF, the probability of filling any deuteron potential orbits in the MC is zero. Near the end of time frame A, the temperature declines and a free electron fills a single empty electron shell in the MC, releasing 15.5 eV of recombination energy. The deuterium ion rapidly increases in volume by eight orders of magnitude ($8\times10^{-38}$ – $8\times10^{-30}$ m$^3$). The increase in volume occurs in 10 fs. A slight delay for cooling of the MC environment permits deuterium ion and electron recombination, forming an SW impulse of high energy density. Figure 13 shows an advantage the MC system has over the muon fusion system, using the 15.5 eV impulse SW within the compressed MC space. This SW fuses two deuterium ions into a single alpha, with heat dissipation in the target foil lattice and surrounding $D_2O$ at the MHz frequencies. As the frequency is reduced more multi-ejecta events are observed [3].

### 5.3. Muon fusion and RF cavitation fusion

The energy density ratios are $10^9$ higher for the deuterons in the MC than the $t\mu + D_2$ reported in muon experiments [20]. The energetic deuterium ions in the MC, with no jet plasma electrons, mix with neutralizing electrons during time frame A to produce a single D atom SW and an alpha. The muon requires more time and energy to substitute a $\mu$ for an electron to produce a large molecular ion decaying to an alpha. Muon experiments use the volume of the combination of $t\mu + D_2$ to produce a $^4$He atom with its orbital electrons. Muon based systems require $10^{-7}$ s to

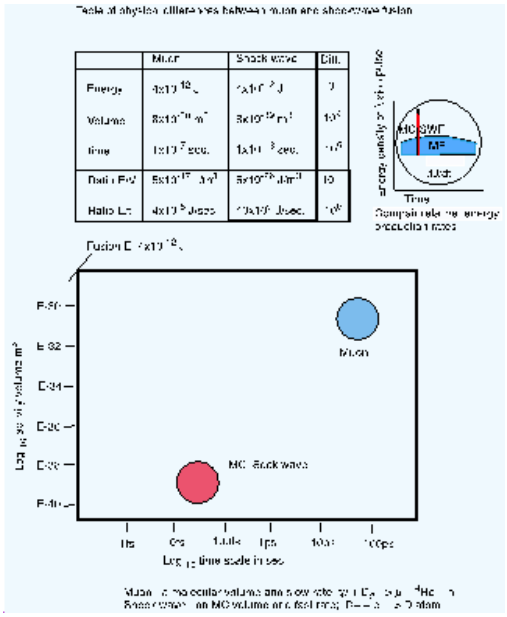


**Figure 12.** Shows a rough comparison of the energy, density, and time scales in a muon fusion event and an MC fusion event. It can be seen that MC events occur in a much smaller volume, and a much shorter time window. The diagram in the upper right of Fig. 12 shows that a high-density energy pulse is associated with MC events, which is conjectured to promote D–D fusion [16–19]. Note the time line spread of the muon fusion pulse event compared to the SW pulse event.

produce a single $^4$He compared to $10^{-13}$ s for the alpha produced by SW fusion.

### 5.4. Photon emission and coupled acoustic pick-up

The SL emissions were measured by various multi pixel devices from a Hamamatsu MPPC 50, 100, and 1600-pixel resolution in a dark box. The average response to SL emission measurements was about 0.05 V shown as blue peaks in Fig. 3. At 1.7 MHz of piezo input, there is a 100 ns SL photon emission cycle (blue peak in Fig. 3) and $1.6 \times 10^6$ photon emissions per cycle calculated from this data that are coupled to the piezo frequency. The same coupled frequency is also found in the PVDF sound detection system showing a beat frequency of a second near-by frequency produced in the target foil (see Fig. 2). The SL measurements were made in a dark box minimizing the background light and cooled by the circulating water passing through the 0.63 MHz piezo device. These systems produced more than a million jet plasma sources per second. In these experiments, a Pd wire 0.0031 in. in diameter was used instead of a target foil with the cylindrical cavitation forces focused along the length of the wire. The piezo device had a 9 mm radius and 17 mm length with an ID of 4 mm.

### 5.5. Meso-cluster of deuterons

Free and highly mobile electrons are implanted in the MC and are influenced by attractive and electromagnetic forces; the electrons compress the MC and the deuterons contained within. At the end of the compression cycle, the MC temperature declines and the probability of recombination in the MC increases. An electron combining to form a neutral D atom produces the SW event. The SW is a high-energy impulse capable of triggering D–D fusion events.

**MS measured helium four**

| Date | RF Sample | cc Volume | Atm. Pressure | He4 PPM | RF Cav. Liquid | Time in min |
|---|---|---|---|---|---|---|
| 05/07/18 | 4 | 50 | 1.3 | 0.363 | D2O | 33 |
| 05/07/14#2 | 4 | 25 | 1.3 | 0.557 | D2O | 33 |
| 04/26/18#2 | 3 | 50 | 1.0 | 0.484 | H2O | 47 |
| 04/26/18 | 3 | 25 | 1.0 | 4.27 | H2O | 47 |
| 04/26/18 | 3 | 25 | 1.0 | 0.996 | H2O | 47 |
| 12/10/16 | 2 | 50 | 1.3 | 0.53±0.1 | D2O | 80 |
| 12/10/16#2 | 2 | 25 | 1.3 | 3.3±0.05 | D2O | 80 |
| 10/15/16 | 1 | 50 | 1.3 | 3.3* | D2O | 80 |

* Two Runs @ 3.3 PPM ~ 1.5% difference

| | | | | | | |
|---|---|---|---|---|---|---|
| 05/21/18 | Ar | 50 | 1.0 | 0.1±0.1 | _Ar | 0 |

Firstgate Ar tank

MS by McFarland Instrument Services

**Figure 13.** Values for the mass spectrometry results for the RF reactor system are tentative; Results from a new mass spectrometer are discussed in a parallel ICCF 21 paper by Tom Claytor, Malcolm Fowler, and Roger S. Stringham.

In summary, the MC is compressed to fusion by reducing the distance between D ions so alpha fusion occurs as in muon fusion. At high cavitation frequencies, there are single or multi fusion events in the target foil and release $3.83\times10^{-12}$ J (24 MeV) of energy per D–D fusion event. The MC is destroyed in this process and its remnants have been detected by mass spectrometry and SEM; they were found to be similar at all applied frequencies and have similar concentration levels [3] reverting back to the $D_2O$, and the steady state $D_2$ and DOOD. The RF cavitation process, with its alpha output, requires about $10^{13}$ fusion events per second from a one $cm^2$ target foil to produce 40 W of anomalous power. Note that the MC event at low frequency, 20 kHz, systems are dominated by large destructive multi events and with some single MC events (basic minimum event is the formation of one alpha). The MHz frequencies are typically single events with a few 2 and 3 FCC ejecta crater events.

### 5.6. Table of MS $^4$He measurements

Mass spectrum measurements by Malcolm Fowler of MIS labs in New Mexico of RF samples delivered from Firstgate Energies lab in Hawaii. .

### 5.7. Structural coloration

Thin oxide colored films are formed on the target foil surface. Ordinary sunlight striking the surface of a target foil that has been exposed to $D_2O$ cavitation may have a high degree of coloration and patterns that are controlled by the input power and frequency of the $D_2O$ cavitation. It is conjectured that the coloration is a result of standing surface waves;

such standing waves are influenced by target foil edge binding during cavitation in the reactor. The TF thickness (generally 100 $\mu$m) is exposed to surface oxidation and the high temperatures influence the color showing standing wave patterns on the TF. The colorations are particularly strong for the BCC titanium target foils. These target foils have no ejecta craters but the exposed surface was highly colored. Run # 17 tested in 1995 consisted of a 5 $cm^2$ and 100 $\mu$m thick foil of titanium. The sample was placed in a 46 kHz cavitating $D_2O$ reactor and secured at four corners of the foil. The exposed foil's surface was colored by an iridescent pattern of a standing wave that covered about 1/3 of the exposed foil. The pattern was geometric repeating and showed a 2-dimensional multi-color square pattern about 3 mm on a side. A zirconium foil showed the same pattern. Ti and Zr are both body-centered cubic metals (BCC). The other three target foils in this sample group were face centered cubic metals (FCC) and showed surface ejecta sites at all frequencies tested. The smallest ejecta site was $\sim$50 nm in diameter and 50 nm deep, and required about $4\times10^{-12}$ J (24 MeV) of energy to form the crater.

From surveys of many SEM photos, FCC target foils showed ejecta damage, but BCC target foils did not. Ti and Zr are BCC metals. There is evidence in the BCC target foils for a multi-layered $TiO_2$ surface build-up and small micron-diameter tubes [8,9]. In cavitation systems, the same tubes are produced but are so delicate they fragment in the cavitation field [12]. The exotic coloration in structured layers found in exposed titanium target foils may derive from the same physics as that which explains the coloration found in oil slicks and bird feathers [21]. The strong coloration is the result of $TiO_2$ thickness on the titanium target foils and shows the 2-dimensional surface pattern in color variation that relates to a build-up of $TiO_2$ via the resonant frequency of the acoustically driven target foil [12]. The surface of BCC titanium is made up layers of titanium oxide, anatase, rutile, and brookite as a mixture. The standing wave alters the thickness of the oxide layers.

### 5.8. Temperature of events

Target foils of a thickness of about 100 $\mu$m, were placed into a cavitating reactor, and depending on the frequency applied to the exterior surfaces, the target foils immediately lost their original surface appearance. This is typical for the start of any cavitation run. When the cavitation operates in the MHz range, the surface crystal structure is melted, cooled and cycled more than a million times per second in the MHz range. At 20 kHz it is possible to observe the surface while running and observe a glistening that will disintegrate the target foil if the power input is too great. This phenomenon is altered by increasing the frequency [3]. This altered target foil surface structure typically changes to a very fine-grained surface in the target foil's active area. During reactor operation, the target foils are slowly changing by forming surface oxides and fine-grained surfaces, where events start at the beginning of the run and continue with the slow destruction of the target foil surface.

Face centered cubic (FCC) target foils continue to lose mass through ejecta sites from the surface of the FCC foil. The bulk of the target foil system is at a steady-state temperature; an isolated event that produces the fusing SW that is in the range of 10,000 K has little effect on the bulk steady-state temperature. Events are made up of about 2–100 charged particles in the MC and are a one-time TF surface event that produces alphas in a self-destructive process. During the particle plasma compression cycle, ejecta craters are formed, and are about 50 nm deep with a 25 nm radius. Measurements from SEM photos and mass spectrometer measurements show alphas only exist near the surface of the target foil. The above statements hold true for the FCC target foils but not for BCC target foils. Titanium target foils produce $^4$He, as detected by mass spectrometry but the $^4$He is found in the bulk and ejecta sites are not observed [1]. At the elevated temperatures produced by high-frequency cavitation, deuterium exists mainly in ionic form. The cavitation process provides continuous rebuilding and recycling of the older target foil surface, maintaining a fresh active surface area on the target foil for D–D reactions.

The palladium TF surface is initially very bright and smooth but after 5 min of cavitation a hole in the surface is often produced at 20 kHz in high-power mode. There are archived videos of this process. When testing palladium

target foils, new surfaces are created and maintain the crater population at steady state, the new destroying the old, while altering the surface of the target foil with each cycle. This process creates a new recrystallized microstructure surface.

The titanium TF surface provides no barrier to the formation of MCs. The TF lattice provides containment of the MC, where the free electrons move toward the deuteron charge center. The MC plasma can be composed of say 10 deuterium ions and N concentric electrons; the MC deuteron sphere in time frame A is driven to charge neutralization.

Charge neutralization powers the compression of the spherical MC. The titanium TF (BCC) shows no surface craters or corresponding ejecta. It does show the same $D_2O$ fragmentation in mass spectrometer measurements of $D_2$ and DOOD [2]. The titanium target foils are observed to have a gray paste adhering to the $TiO_2$ foil surface. The gray paste may be associated with the presence of alpha products, $^4$He, and heat; the heat was dispersed through the 100-$\mu$m thick TF, cooled by the circulating $D_2O$.

It is the free electron mobility in time frame A when the ideal conditions in the MC are passed through that produces one neutral D atom, the 15.5 eV shockwave, a fusion impulse, and one alpha. During cavitation, this process can produce $10^{13}$ reactions per second, generating measurable and useful heat. This is the MC.

## 6. Conclusion and Summary

A good place to start is a paper that appeared in 1986 by A. Henglein Sonochemistry review, ultrasonic Vol. 25, 1987. His MS analysis confirmed the presence of the two markers $D_2$ and DOOD following $D_2O$ cavitation; these markers were present from the very beginning of the measurements made in this 1986 mass spectrometry system. The markers were measured using mass spectrometer analysis of RF cavitation in Ar-saturated $D_2O$ and were collected in gas samples that revealed their measured masses of 4 and 20 [2]. The markers in the Ar -saturated $D_2O$ were in a steady state concentration.

The newer RF technology showed that at $\sim$2 MHz, $^4$He was produced in 20 and 80 min experiments, without a good correlation of the produced heat as shown in Fig. 6. The emphasis was on the measurements for $^4$He but the measurements do show a general correlation with evolved heat.

The RF technology is new but 2 years of work with Ar-saturated $H_2O$ systems and solving RF interference problems preceded the experiments using $D_2O$. An RF duty cycle for reactor operation during both the active and calibration experiments was developed; measurements were made with the RF in off-mode to eliminate RF interference. The RF duty cycle was 30 s on, 5 s off. During the 5 s off period, reliable $\Delta T$ measurements were made. The duty-cycle method was adopted to make temperature measurements possible in the active RF reactor.

The advantage of the RF system was that you can use the 50-watt audio amplifier for a wide range of tunable frequencies at high amplitudes. The system was tuned by adjusting parameters to minimize the SWR, keeping it below 1.20. The reflected RF wave input should be minimized.

Samples of cavitation products were collected at the end of each run with vacuum transfer of 50 and 25 ml sample bulbs and were sent to the laboratories of Tom Claytor and Malcolm Fowler near LANL in NM. Experiment RF four $D_2O$ and Pd was conducted on April 19, 2018; samples were taken and analyzed for tritium and $^4$He. Figures 6 and 7 show the details of a typical analysis. The MS analysis, as mentioned in Fig. 7, showed the expected markers for the Ar-saturated $D_2O$ cavitation and had a presence at all cavitation frequencies that were used. These RF systems heated water to steady state after about 1000 s with the heat exchange system in place (Fig. 4b). Heat was removed until heat-in equaled heat-out. Heat-in and heat-out were in balance via the two Cu coils. One coil was in the $D_2O$ and the other coil was in the 3.5-liter $H_2O$ reservoir, an isolated cooling system. The reactor temperature was kept at steady-state temperature (Fig. 4b). The acrylic reactor, while running, lost surface mass at the cavitating $D_2O$-acrylic interface; acrylic fragments were identified by the MS analysis (see MS graph Fig. 7).

One system that was run in a dark box and used Hamamatsu MPPC devices focused on the SL emission mea-

surements. In these runs at approximately 1 MHz of acoustic input, the active period was about 100 ns and the MC population pulse was spread over the active period during one acoustic cycle of 1.7 MHz. The rest of the time the system was inactive (see Fig. 3). This information can be used to estimate a maximum frequency for the bubble collapse mechanism.

In two cases, the $^4$He measurements revealed either a concept failure or a $^4$He removal failure. Two runs (RF 3 $H_2O$ and Pd and RF 4 $D_2O$ and Pd) measured $^4$He, as shown in Fig. 13; measurements showed $^4$He in light water and heavy water samples. These amounts were less than the $^4$He concentration in atmospheric air. The saturated Ar-$D_2O$ systems used Argon from a tank that was measured at 0.02 ppm of $^4$He.

At the start of the experiment using light water ($H_2O$), distilled water was added to the RF reactor and was vacuum-pumped to remove all air bubbles from the RF reactor; this was the exact protocol used in the heavy water ($D_2O$) experiments. The only bubbles visible at the end of the pumping sequence were large $H_2O$ vapor bubbles. At this point, argon was added to 1 atm. and the experiment proceeded along the normal path. The samples were collected and delivered to Claytor and Fowler. The mass spectrometry in this case was not as impressive as the $^4$He measurements made by Brian Oliver of PNNP [1]. The light-water based RF Sonofusion samples showed as much or more $^4$He than the heavy-water based RF experiments.

A comparison was made between the muon catalyzed fusion rate producing $^4$He in its fusion process of $\mu$ capture or catalysis [7] to the RF, the mechanism rate that produces the SW that fuses two deuterons producing an alpha. The relative rates of RF and $\mu$ catalyzed fusion show that the RF fusion rate is millions of times faster and should be more successful (see Fig. 12). I am sure mass spectrometer measurements will improve and advance the cavitation know-how for control of alpha production and show if this is a fruitful path to a future that controls $^4$He output and heat capture.

## References


[1] R. Stringham, Helium measurements from target foils, LANL and PNNL, 1994, *J. Condensed Matter Nucl. Sci.* **24** (2017) 284–295.

[2] R. Pflieger, T. Chave, M. Virot and S.I. Nikitenko, Activating molecules, ions, and solid particles with acoustic cavitation, *J. Vis Exp.* **86** (2014) 51237.

[3] R.S. Stringham When bubble cavitation becomes sonofusion, *J. Condensed Matter Nucl. Sci.* **6** (2012) 1–12.

[4] URL retrieved from <http://nct resource center, FCC and BCC crystallography of metals>, 2018.

[5] P.A. Mante, M. Anttu, W. Zang, J. Wallentin, IJ. Chen, S. Lehmann, M. Heurlin, M.T. Borgstorm, M.E. Pistol and A. Yartsev, Confinement effects on Brillouin scattering in semiconductor nanowire phonic crystal, Department of Chemical Physics and Lund University, Swenden, APS.

[6] Isotopic data for boron and its isotopes is found in the Periodic Table.

[7] K. Nagamine, *Introductory Muon Science*, Cambridge University Press, Cambridge, 2003.

[8] C.M. Wen, N. Uekawa, K. Khamfoo and T. Kjimao, Titanium oxide thin film preparation with sol coatings of plate and spindle-shaped nanoparticles for control of optical transmittance, *J. Ceramic Soc. Japan* **124** (1) 60–65.

[9] N.J.R. Zhang, Y. Chen, H. Wu, W. Chen, C. Zhao and X. Zhang (2016), Study of cell behaviors on anodized $TiO_2$ nanotube arrays with different structures, FBIOE.2016.01.01130, Mar. 2016.

[10] V.V. Zheleznov, E.I. Voit, Y.V. Sushkov, S..A Sarin, V.G. Kuryavyi, D.P. Opra, S.V. Gnedenkov, S..L Sinebryukhov and A.A. Sokolov and A.A. Sokolov, Nanostructured microtubes based on $TiO_2$ doped by Zr and Hf oxides with the anatase structure, *IOP Conf. Ser.: Mater. Sci. Eng*., 11201, 2016.

[11] P.J.E. Peebles, Recombination of the primeval plasma, *Astrophy. J.* **153** (1968) 1.

[12] R.S. Stringham, Sonofusion produces tritium that decays to helium three, *Proc ICCF 15*, V. Violante and F. Sarto (Eds.), Oct. 5–9, 2009, p. 57, Some parts need a rewrite.

[13] Changing with increasing T$\alpha$ phase of Ti is dominant and BCC changing from the $\beta$ phase HPC, BCC and BCC.

[14] Julius Su and A William, Goddard III (advisor), An electron force field for simulating large scale excited electron dynamics,

Caltech, Thesis, 2008.
[15] R.S. Stringham, Conservation of E and M, single cavitation heat events *J. Condensed Matter Nucl. Sci.* **15** (2015) 55.
[16] K. Nagamine, *Introductory Muon Science*, Cambridge University Press, Cambridge, 2003, p. 79.
[17] Phillip Ball, We choose to go to the muon, Chemistry World, 2014.
[18] C.R. Nave, HyperPhysics, Muon Experiment, 2014.
[19] C.R. Nave, HyperPhysics, Atmospheric Muons, 2014.
[20] K. Nagamine, *Introductory Muon Science*, Cambridge University Press, Cambridge, 2003, p. 71.
[21] A.R. Parker and N. Martini, Structural color in animals – simple to complex optics, *Optics Laser Technol* **38** (4–6) (2006) 19.